OPEN ACCESS

Dynamics of graphene growth on a metal surface: a time-dependent photoemission study

New Journal of Physics
The open-access journal for physics

Dynamics of graphene growth on a metal surface: a time-dependent photoemission study

Alexander Grüneis[1,2,4], Kurt Kummer[3] and Denis V Vyalikh[3]

[1] Faculty of Physics, University of Vienna, Boltzmanngasse 5, A-1090 Vienna, Austria
[2] IFW Dresden, PO Box 270116, D-01171 Dresden, Germany
[3] Institute of Solid State Physics, Dresden University of Technology, D-01062 Dresden, Germany
E-mail: alexander.grueneis@univie.ac.at

New Journal of Physics **11** (2009) 073050 (9pp)
Received 20 April 2009
Published 29 July 2009
Online at http://www.njp.org/
doi:10.1088/1367-2630/11/7/073050

Abstract. Applying time-dependent photoemission we unravel the graphene growth process on a metallic surface by chemical vapor deposition (CVD). Graphene CVD growth is in stark contrast to the standard growth process of two-dimensional films because it is self-limiting and stops as soon as a monolayer of graphene has been synthesized. Most importantly, a novel phase of metastable graphene was discovered that is characterized by permanent and simultaneous construction and deconstruction. The high quality and large area graphene flakes are characterized by angle-resolved photoemission, proving that they are indeed monolayer and cover the whole 1×1 cm Ni(111) substrate. These findings are of high relevance to the intensive search for reliable synthesis methods for large graphene flakes of controlled layer number.

Its astonishing electronic properties have placed graphene, a planar sheet of carbon atoms packed in honeycomb structure, in the focus of considerable current research efforts [1, 2]. The occurrence of Dirac fermions at low energies and the remarkably high electron mobility have raised high expectations regarding its future use as an active element in nanoelectronics and hybrid materials. Moreover, graphene is highly promising to play a crucial role in future spintronic applications and can serve as an effective oxidation protection when grown epitaxially on metal surfaces [3].

[4] Author to whom any correspondence should be addressed.

Naturally these findings have stimulated the development of efficient and reliable synthesis protocols for high-quality graphene layers. To date several techniques have been established: (i) precipitation from silicon carbide [4], (ii) mechanical exfoliation from graphite [1, 5], (iii) reduction of exfoliated graphite oxide [6]–[8], (iv) thermal expansion of graphite oxide [9], (v) laser desorption [10] and (vi) growth by chemical vapor deposition (CVD) on metal surfaces [11]–[14]. The latter is especially interesting for ferromagnetic materials and it was demonstrated that spin polarization of a Ni(111) substrate can be cloned almost completely into a graphene overlayer [15]. This allows to design sources of spin polarized electrons that are fully prevented from ageing when exposed to reactive gases. Despite these promising perspectives, little is known about the actual growth mechanism of graphene on metal surfaces [16].

Here, we show that the high spatial compatibility of the Ni(111) surface and the graphene sheet makes it a perfect system to study functional synthesis of monolayer graphene on metal substrates by a self-limiting CVD process. The high crystallinity and quality and large area growth of monolayer graphene are unambiguously proven by low energy electron diffraction (LEED) and angle-resolved photoemission spectroscopy (ARPES) of the electronic band structure. For CVD of the graphene layer, a freshly prepared Ni(111) substrate was heated and stabilized at the desired synthesis temperature first. Then propylene gas (C_3H_6), which served as the carbon source, was introduced into the chamber. Doing so the gas pressure was adjusted to 2×10^{-7} mbar using a leak valve. In the incipient reaction of propylene with the Ni surface, a graphene monolayer is formed as evidenced by the appearance of a single π band by ARPES as will be shown later. During the whole synthesis procedure the C 1s signal was recorded together with the C_3H_6 gas pressure and the substrate temperature. This complete set of information allowed us to monitor the full growth process dependent on time. The C 1s spectra were recorded at $h\nu = 400$ eV photon energy. The Fermi level position was measured at least twice for each experiment providing a reference point for the measured core level peaks.

One time-dependent data set recorded during the graphene CVD is shown in figure 1. Starting from a blank Ni film kept at room temperature, it shows the time evolution of (a) the raw photoemission (PE) signal in the C 1s range, (b) the C_3H_6 partial pressure, (c) and (d) the C 1s signal intensity integrated for a range of ± 0.5 eV around the blue and green lines in (a), respectively. Considering the C 1s spectra, it is evident that in the beginning the prepared Ni(111) surface still shows small signs of carboneous contaminations at 283 eV binding energy (BE). They, however, are fully removed during the first 200 s when the substrate temperature is raised to the synthesis temperature for the graphene growth. After the substrate is stabilized in temperature the leak valve to the C_3H_6 gas inlet is opened (this point corresponds to a time $t \sim 500$ s). Immediately with increasing C_3H_6 pressure a distinct peak at 283 eV BE arises. Only at $t \sim 600$ s does the graphene related peak at 284.7 eV start to grow. The dashed vertical lines in figures 1(b)–(d) indicate the opening of the valve to the C_3H_6 gas inlet and the start of graphene growth, respectively. The completion of a graphene layer is evidenced by the saturation of the C 1s peak and LEED (see inset of figure 1(a)). We wish to point out here that such a sharp hexagonal LEED pattern is proof of the 1×1 reconstruction and a good case for the successful CVD synthesis of graphene; if the CVD did not yield graphene, the LEED pattern showed many irregular spots and a high background intensity. Note that for this synthesis temperature the sample can be cooled down anytime after the graphene layer is complete (i.e. $t > 800$ s) without inducing a change in the graphene layer, i.e. all PE spectra remained unchanged. Concerning the temperature stability during the exposure to C_3H_6 gas, the massive single crystal substrate that

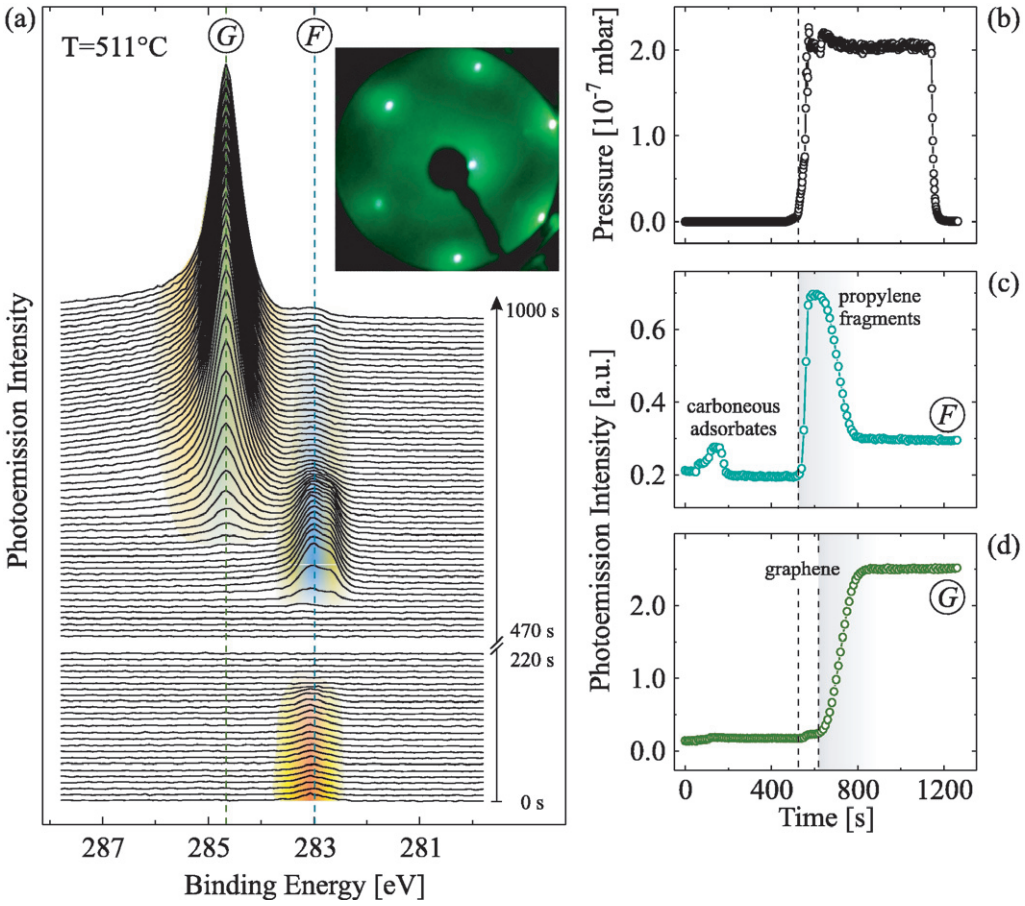

Figure 1. (a) Time evolution of the PE intensity in the C 1s region during the graphene growth. Individual scans were taken every ten seconds. *F* and *G* mark the signals from C_3H_6 fragments and graphene. The inset shows a LEED pattern (primary energy was 80 eV) after growth of graphene. (b) Partial C_3H_6 pressure. (c) and (d) Intensity of the fragment and the graphene C 1s PE signal integrated over ± 0.5 eV around their peak maximum. The dashed vertical lines in (b)–(d) indicate the start of the exposure to C_3H_6 and the start of graphene growth, respectively.

is in thermal contact with the manipulator prevents the sample from cooling down. This fact is also evidenced from the constant temperature measured at the backside of the crystal. Although we can expect some variation with respect to the surface temperature, we believe that this effect is negligible with respect to the growth processes described here.

Three origins of the 283 eV peak are conceivable: (i) unfragmented C_3H_6, (ii) surface nickel carbide and (iii) C_3H_6 fragments. The former two, however, are not supported by additionally performed experiments. Firstly, producing a C_3H_6 film on Ni(111) by room temperature adsorption we found the C 1s PE peak at $\sim$284 eV BE and not at 283 eV BE (not shown). Secondly, we have deliberately synthesized nickel carbide and proved this by LEED as described previously [17]. We indeed detected the C 1s peak at 283 eV BE, in agreement with literature values [18] for nickel carbide. But we were not able to convert the surface nickel carbide film into graphene by heating. Instead we observed that the nickel carbide film is stable

and the peak at 283 eV did not vanish nor did a graphene peak appear. Thus, we conclude that the observed peak at 283 eV BE is due to C_3H_6 fragments and in agreement to previous work that reports a very similar experiment of carbon monoxide decomposition on Rh, we assign it partly to atomic carbon [19]. Another contribution to this peak might be edge atoms of the growing graphene film. Indeed, this would explain why the intensity decreases as the graphene layer forms and has fewer edge atoms. Our assignment is also consistent with the fact that we did not observe any sign of C–H bonds, which appear as a sideband in the C 1s peak at $\sim$1 eV higher BE than the graphene peak [20].

Looking at figures 1(c) and (d) one recognizes that during construction of the graphene network a major part of the fragments vanishes, i.e. it is transformed into graphene. From the time dependence it is also likely that fragments are only produced up to a critical coverage and that no more fragments are produced after the fragment peak has reached its maximum. This is also evident from the fact that the rate of fragment production decreases already before graphene is formed. When the graphene growth is completed only a minor fraction of fragments remain. For all recorded spectra, the beginning of both the graphene peak rise and the fragment peak maximum coincide in time. Comparing the maximum intensity of the fragment peak ($\sim$0.7 a.u., figure 1(c)) and graphene peak ($\sim$2.5 a.u., figure 1(d)) it becomes apparent that there is an additional path of carbon incorporation to achieve a complete monolayer. This path does not obviously show up in the core level spectra of the fragments on the surface. Thus we speculate that C incorporation into graphene is possible following the dissociation of C_3H_6 at the graphene edges. Such a process corresponds to growth from the gas phase; it is conceivable because the edges of the growing graphene possess a catalytic activity.

The percentage of fragments in the final graphene layer depends considerably on the synthesis temperature as shown in figure 2(a). While clearly present for lower synthesis temperatures a distinct fragment peak is not observed beyond $\sim$600 °C. This highlights that high temperatures result in an efficient conversion of fragments to graphene. The quantitative comparison of the fragment PE and the graphene PE intensities in figure 2(b) reveals a decline in their ratio from 10% to about 1% when going from 345 to 669 °C. The high structural quality of the graphene layer synthesized at 669 °C is confirmed by least-squares fit analysis of the C 1s PE spectrum. Using a single component with Doniach–Sunjic lineshape, we obtained a peak position at 284.7 eV and $\Gamma_l = 216$ meV and $\alpha = 0.1$ for the intrinsic line width and asymmetry parameter, respectively, which is in agreement with previously reported values [14].

The synthesis temperature is decisive not only for the structural quality of the graphene layer, it furthermore governs the graphene growth rate. In figure 3(a), the time evolution of the graphene PE intensity is shown for increasing temperatures. For the purpose of comparison, the curves were aligned with one another on the timescale. Taking the slope of the C 1s intensity of graphene at the turning point of the curve as a measure for the growth rate we found that the latter has a synthesis temperature dependence as shown in figure 3(b). For temperatures below 350 °C no extensive graphene growth occurs. Then a rapid increase in the growth rate is observed when the synthesis temperature is raised to about 500 °C. Beginning from 500 °C the growth rate remains constant before it appears to decline again above 650 °C. In contrast to graphene layers synthesized at lower temperatures, we found that those constructed at 657 and 669 °C exist only in a metastable phase.

In figure 3(c), we show a full data set of propylene pressure and fragment and metastable graphene C 1s PE intensities for $T = 669$ °C. The important point in these experiments is the fact that at these elevated temperatures graphene only exists as long as carbon is supplied; the

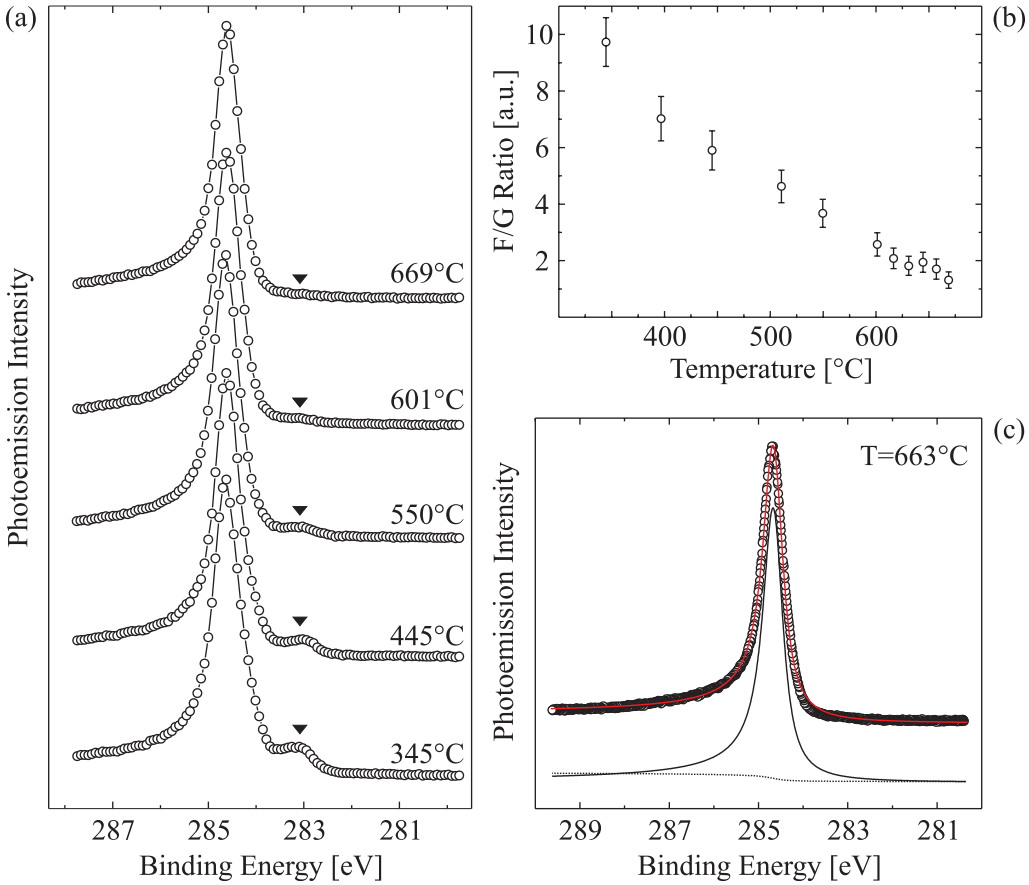

Figure 2. (a) C 1s PE spectrum of the fully grown graphene layer for different temperatures. (b) Fragment to graphene PE intensity ratio as a function of synthesis temperature. (c) High resolution C 1s spectrum for graphene on Ni(111) along with a Doniach–Sunjic lineshape analysis. The red line denotes the fit to the experimental data (see text for fit parameters).

graphene PE signals disappear as soon as the carbon supply is cut off. Note that the sample temperature remains unchanged during the whole experiment. When propylene is introduced into the chamber the graphene grows up to completion of one monolayer. From figure 3(c) it can be seen that a closed graphene layer is reached at $t \sim 400$ s. The gas inlet is closed at $t \sim 600$ s (indicated by a dashed vertical line) and immediately thereafter the graphene C 1s intensity decreases. The graphene layer PE signal completely disappears within 400 s after the carbon supply has been turned off. Note that graphene only disappears if the temperature is high as described above. For the case of lower temperature synthesis (such as the one shown in figure 1), the graphene layer does not desorb if the gas inlet is closed.

Two possible reasons for the disappearance of graphene carbon atoms are conceivable. Firstly, it may be possible that at such high temperatures carbon atoms in graphene react with residual gases in the chamber, e.g. hydrogen, and form hydrocarbons that can easily desorb. Secondly, diffusion of carbon atoms into the bulk Ni could set in for the highest applied temperatures [21]–[23]. The question of whether desorption or diffusion is dominating remains subject to further investigations. We wish to point out that after high-temperature deconstruction

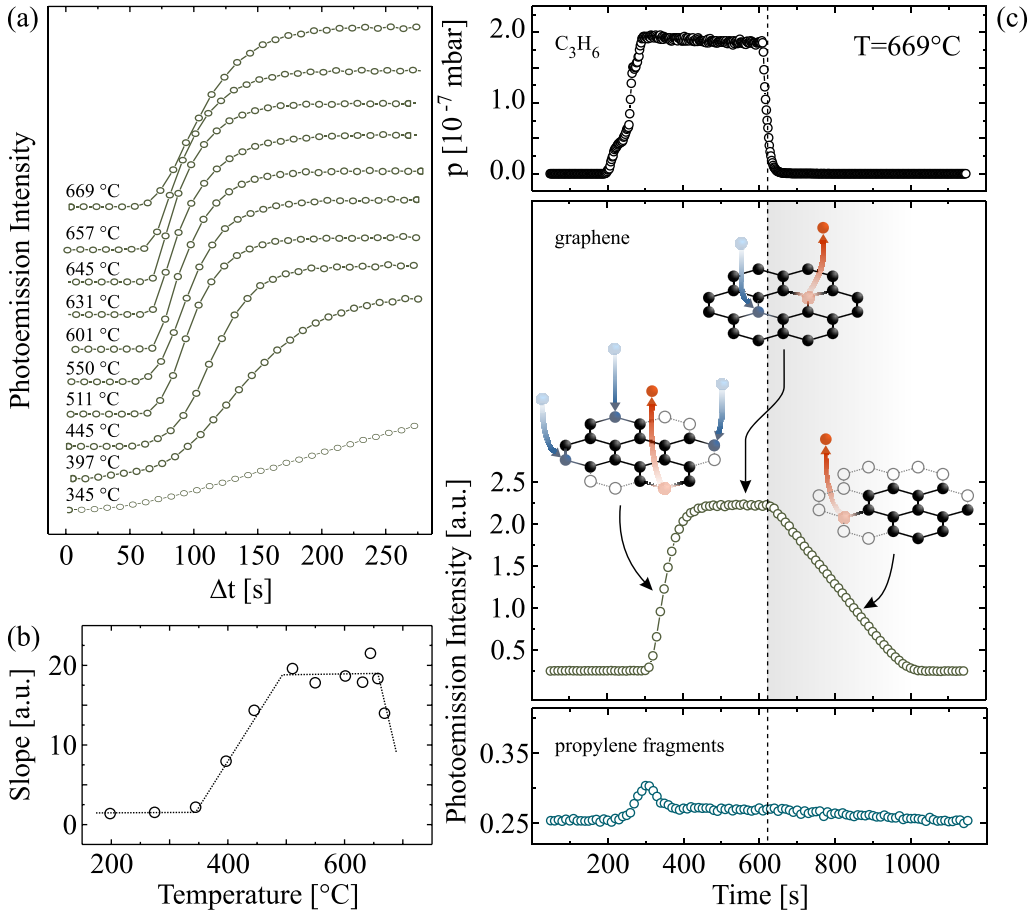

Figure 3. (a) Time evolution of the graphene C 1s intensity for different temperatures. (b) Graphene growth rate as a function of synthesis temperature. (c) Graphene C 1s intensity spectrum for $T = 669\,^{\circ}\mathrm{C}$ indicating three consecutive development stages: rapid growth, a metastable phase and desorption or diffusion. The dashed vertical line indicates the closing of the valve to the C_3H_6 inlet, i.e. the end of exposure of the Ni(111) surface to C_3H_6.

of the graphene layer no notable amount of carbon remains on the surface. In fact, after repeated synthesis and heating procedures we always found a pristine Ni surface, ready for a new cycle of graphene growth.

Finally, we demonstrate the high quality of a graphene monolayer synthesized at 550 °C by performing a mapping of the electronic band structure using ARPES. All ARPES spectra were acquired at a photon energy of $h\nu = 40.8\,\mathrm{eV}$ and the binding energies were determined with respect to the Fermi edge. The measured band structure between Γ and K points in the two-dimensional Brillouin zone is shown in figure 4(a). The appearance of π and σ bands is a clear indication for the long-range electronic order. Furthermore, a gap at the K point appears, which is a result of substrate interaction and hybridization of C $2p_z$ and Ni $3d_{3z^2-r^2}$ orbitals as discussed previously [11]. The region of the gap is marked by a rectangle in figure 4(a). In figure 4(b), the corresponding raw spectra are depicted as energy dispersion curves (EDCs) for different emission angles. The EDC that passes through Γ and K points at the Fermi energy are depicted

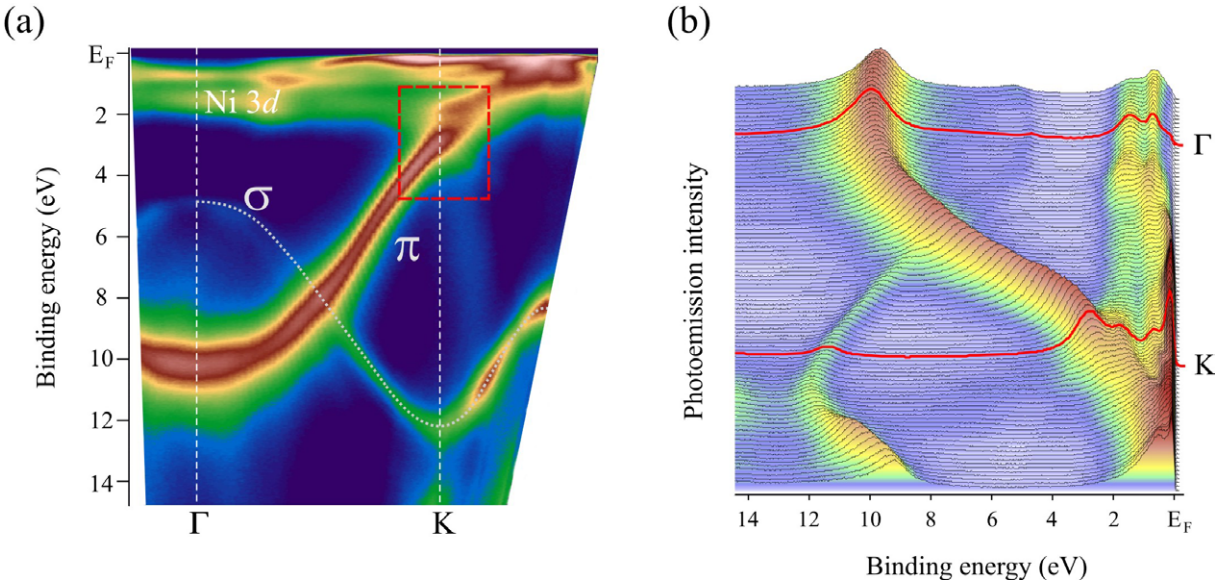

Figure 4. (a) Band structure mapping by ARPES of a graphene monolayer synthesized at 550 °C. The graphene derived π and σ bands and the Ni 3d bands are depicted. The region around K denoted by a dashed rectangle exhibits the gap in the π band structure, which is due to substrate interaction. (b) The raw ARPES spectra: red lines denote scans taken at Γ and K points, respectively.

in red. It can be seen from the ARPES results that only one π valence band is visible. This demonstrates unambiguously that we have indeed synthesized monolayer graphene because the number of π bands in a graphene N-layer would be equal to N. For example, our tight-binding calculations indicate that bilayer graphene has two π bands that are separated by ∼0.4 eV [24]. Thus, the appearance of only one π band in the ARPES spectra also strongly supports the observation from the time-resolved PE that the catalytic activity diminishes after the growth of one monolayer. (See the C 1s core level spectra intensities that saturate once a graphene monolayer is formed as shown in figure 1(d).) Indeed the growth of a second graphene layer on top of the first is not possible for the same synthesis temperature and C_3H_6 pressure that was used to grow the first graphene layer in contact with the Ni(111) surface. This is due to the fact that the active Ni sites are covered with carbon atoms that have a low catalytic activity if they are bonded in a hexagonal arrangement with three nearest neighbours.

In summary, applying time-resolved PES we were able to observe and characterize the dependence of graphene quality and growth rate on the synthesis temperature, for the first time. For high temperatures above 650 °C, we found the graphene layer to be in a metastable state characterized by permanent simultaneous construction and deconstruction. The high crystallinity and quality of the synthesized graphene monolayers was confirmed by LEED and a mapping of the electronic band structure by ARPES.

Acknowledgments

AG acknowledges an APART fellowship from the Austrian Academy of Sciences and a Marie Curie Individual Fellowship (‘COMTRANS’) and travel support from the EU. DV acknowledges the Deutsche Forschungsgemeinschaft (Grant VY 64/1-1). We are grateful

to A Goldoni, S Lizzit and P Vilmercati for their support at the SuperESCA beamline and to R Hübel for his support at the IFW-Dresden.

Appendix. Experimental details

The substrate was a W(110) single crystal that could be heated from the backside by electron bombardment or a filament. The temperature was monitored at all times using a thermocouple that was spot welded on the back side of the tungsten crystal to ensure good thermal contact. The W(110) surface was cleaned by repeated cycles of short flashes up to 1700 °C and annealing in oxygen at 1000 °C. Subsequently, a Ni film of 10 nm thickness was deposited on the W(110) surface by electron beam evaporation from a Ni rod (99.9% purity). The Ni film thickness was monitored by a quartz microbalance. During Ni deposition the tungsten crystal was heated to a constant 150 °C from the backside. Nickel grows epitaxially in (111) fashion on W(110) [25] and we further employ it as a catalytic template for graphene CVD due to its small lattice mismatch. LEED and photoelectron spectroscopy (PES) were utilized to check the W(110) and Ni(111) surfaces for order and cleanliness [11, 25]. For all experiments, the base pressure before dosing C_3H_6 was better than 5×10^{-10} mbar, during Ni evaporation better than 2×10^{-9} mbar. Time-dependent experiments were carried out while dosing 2×10^{-7} mbar of C_3H_6 at the SuperESCA beamline of the ELETTRA synchrotron (Trieste, Italy). The C 1s spectra were recorded at $h\nu = 400$ eV photon energy. The total experimental resolution was ~180 meV and the spot size on the sample was $200 \times 30\,\mu$m. The electronic band structure was measured with ARPES at the IFW-Dresden using a PE spectrometer equipped with a Scienta SES-200 hemispherical electron-energy analyzer and a high-flux He-resonance lamp (Gammadata VUV-5010). All ARPES spectra were acquired at a photon energy of $h\nu = 40.8$ eV (He IIα) with an angular resolution of 0.3° and a total-system energy resolution of 50 meV.

References

[1] Novoselov K S, Geim A K, Morozov S V, Jiang D, Zhang Y, Dubonos S V, Grigorieva I V and Firsov A A 2004 *Science* **306** 666
[2] Geim A K and Novoselov K S 2007 *Nat. Mater.* **6** 183
[3] Dedkov Y, Fonin M, Rüdiger U and Laubschat C 2008 *Appl. Phys. Lett.* **93** 022509
[4] Seyller T *et al* 2006 *Surf. Sci.* **600** 3906
[5] Xiaolin L, Guangyu Z, Xuedong B, Xiaoming S, Xinran W, Enge W and Dai H 2008 *Nat. Nanotechnol.* **3** 538
[6] Niyogi S, Bekyarova E, Itkis M E, McWilliams J L, Hamon M A and Haddon R C 2006 *J. Am. Chem. Soc.* **128** 7720
[7] Gilje S, Han S, Wang M, Wang K L and Kaner R B 2007 *Nano Lett.* **7** 3394
[8] Stankovich S, Dikin D A, Dommett G H B, Kohlhaas K M, Zimney E J, Stach E A, Piner R D, Nguyen S T and Ruoff R S 2006 *Nature* **442** 282
[9] Schniepp H, Li J-L, McAllister M, Sai H, Herrera-Alonso M, Adamson D, Prud'homme R K, Car R, Saville D and Aksay I 2006 *J. Phys. Chem.* B **110** 8535
[10] Rader H, Rouhanipour A, Talarico A, Palermo V, Samori O and Mullen K 2006 *Nat. Mater.* **5** 276
[11] Grüneis A and Vyalikh D 2008 *Phys. Rev.* B **77** 193401
[12] Nagashima A, Tejima N and Oshima C 1994 *Phys. Rev.* B **50** 17487
[13] Gamo Y, Nagashima A, Wakabayashi M and Oshima C 1997 *Surf. Sci.* **374** 61
[14] Preobrajenski A B, Ng M L, Vinogradov A S and Martensson N 2008 *Phys. Rev.* B **78** 073401

[15] Karpan V M, Giovannetti G, Khomyakov P A, Talanana M, Starikov A A, Zwierzycki M, van den Brink J, Brocks G and Kelly P J 2007 *Phys. Rev. Lett.* **99** 176602
[16] Loginova E, Bartelt N C, Feibelman P J and McCarty K F 2008 *New J. Phys.* **10** 093026
[17] Tanaka K and Hirano H 1992 *Catal. Lett.* **12** 1
[18] Kovács Gy J, Bertóti I and Radnóczi G 2008 *Thin Solid Films* **516** 7942
[19] Mongeot F, Toma A, Molle A, Lizzit S, Petaccia L and Baraldi A 2006 *Phys. Rev. Lett.* **97** 056103
[20] Nikitin A, Ogasawara H, Mann D, Denecke R, Zhang Z, Dai H, Cho K and Nilsson A 2005 *Phys. Rev. Lett.* **95** 225507
[21] Siegel D J and Hamilton J C 2003 *Phys. Rev.* B **68** 094105
[22] Lander J, Kern H and Beach A 1952 *J. Appl. Phys.* **23** 1305
[23] Diamond S and Wert C 1967 *Trans. Metall. Soc. AIME* **239** 705
[24] Grüneis A *et al* 2008 *Phys. Rev.* B **78** 205425
[25] Kämper K-P, Schmidt W, Güntherodt G and Kuhlenbeck H 1988 *Phys. Rev.* B **38** 9451